Published in final edited form as:
Mol Imaging Biol. 2010 October ; 12(5): 530–538. doi:10.1007/s11307-009-0284-2.

^{18}F-Labeled Galacto and PEGylated RGD Dimers for PET Imaging of $\alpha_v\beta_3$ Integrin Expression

Shuanglong Liu[1], **Zhaofei Liu**[1], **Kai Chen**[1], **Yongjun Yan**[1], **Petra Watzlowik**[2], **Hans-Jürgen Wester**[2], **Frederick T. Chin**[1], and **Xiaoyuan Chen**[1]

[1] Molecular Imaging Program at Stanford (MIPS), Department of Radiology and Bio-X Program, Stanford University School of Medicine, 1201 Welch Rd., P095, Stanford, CA, 94305-5484, USA

[2] Department of Nuclear Medicine, Klinikum Rechts der Isar, Technische Universität München, Munich, Germany

Abstract

Purpose—*In vivo* imaging of $\alpha_v\beta_3$ has important diagnostic and therapeutic applications. ^{18}F-Galacto-arginine–glycine–aspartic acid (RGD) has been developed for positron emission tomography (PET) imaging of integrin $\alpha_v\beta_3$ expression and is now being tested on humans. Dimerization and multimerization of cyclic RGD peptides have been reported to improve the integrin $\alpha_v\beta_3$-binding affinity due to the polyvalency effect. Here, we compared a number of new dimeric RGD peptide tracers with the clinically used ^{18}F-galacto-RGD.

Procedures—RGD monomers and dimers were coupled with galacto or PEG_3 linkers, and labeled with ^{18}F using 4-nitrophenyl 2-^{18}F-fluoropropionate (^{18}F-NFP) or *N*-succinimidyl 4-^{18}F-fluorobenzoate as a prosthetic group. The newly developed tracers were evaluated by cell-based receptor-binding assay, biodistribution, and small-animal PET studies in a subcutaneous U87MG glioblastoma xenograft model.

Results—Starting with ^{18}F-F^-, the total reaction time for ^{18}F-FP-SRGD2 and ^{18}F-FP-PRGD2 is about 120 min. The decay-corrected radiochemical yields for ^{18}F-FP-SRGD2 and ^{18}F-FP-PRGD2 are 52±9% and 80±7% calculated from ^{18}F-NFP. Noninvasive small-animal PET and direct tissue sampling experiments demonstrated that the dimeric RGD peptides had significantly higher tumor uptake as compared to ^{18}F-galacto-RGD.

Conclusion—Dimeric RGD peptide tracers with relatively high tumor integrin-specific accumulation and favorable *in vivo* kinetics may have the potential to be translated into clinic for integrin $\alpha_v\beta_3$ imaging.

Keywords

RGD dimer; Integrin $\alpha_v\beta_3$; Small-animal PET; Polyvalency

Introduction

Integrins are cell surface receptors responsible for the regulation of cellular activation, migration, proliferation, survival, and differentiation. They possess large extracellular and short cytoplasmic domains. Cytoplasmic proteins with the actin filament of the cytoskeleton are connected with the C-terminal ends of the β-subunit of integrins. These connections play

Correspondence to: Xiaoyuan Chen; shawchen@stanford.edu.
Shuanglong Liu and Zhaofei Liu contributed equally to this work.

an important role in both the outside-in and the inside-out signal transduction pathways. One of the most important members of this receptor class is integrin $\alpha_v\beta_3$, which is involved in many pathological processes [1–3]. Numerous studies showed that integrin $\alpha_v\beta_3$ is necessary for the formation, survival, and maturation of blood vessels. Therefore, its expression level is correlated with the invasiveness of several cancer types, including melanoma, glioma, ovarian, and breast cancers [4–6]. Great efforts have been made to develop $\alpha_v\beta_3$ imaging agents that can visualize and quantify integrin $\alpha_v\beta_3$ expression level [7–9]. Because arginine–glycine–aspartic acid (RGD) peptides could strongly bind to integrin $\alpha_v\beta_3$, many probes have been developed for multimodality imaging of integrin expression based on this RGD peptide sequence [10,11]. These compounds showed high $\alpha_v\beta_3$ affinity *in vitro* and receptor-specific tumor uptake *in vivo*. For positron emission tomography (PET) imaging, Haubner et al. [12] optimized the pharmacokinetics of radiolabeled c(RGDyV) by carbohydration, resulting in ^{18}F-galacto-RGD in which the cyclic RGD peptide monomer c(RGDfK) was coupled with a galacto sugar amino acid (SAA) and labeled with ^{18}F through ^{18}F-2-fluoropropionate. The SAA-linker was inserted to increase the hydrophilicity and consequently improve the pharmacokinetics of the peptide tracer. ^{18}F-Galacto-RGD has now been successfully translated into clinic to image integrin expression in cancer and other disease types [13–20].

The receptor-binding affinity and specificity, hydrophilicity, molecular size, and overall molecular charges of the radiotracers play important roles in radionuclide imaging of integrin expression *in vivo*. Several groups including us found that multimeric RGD peptides have much higher integrin affinity and, thus, significantly improved tumor-targeting efficacy over the monomeric RGD analogs [21–29]. In this study, we derivatized a number of dimeric RGD peptides with SAA and PEG_3 spacers for ^{18}F labeling via 4-nitrophenyl 2-^{18}F-fluoropropionate (^{18}F-NFP) or *N*-succinimidyl 4-^{18}F-fluorobenzoate (^{18}F-SFB) prosthetic group. The goals of this study were to evaluate *in vivo* pharmacokinetics of ^{18}F-labeled galacto-RGD and PEGylated RGD dimers and compare those with the clinically used ^{18}F-galacto-RGD.

Materials and Methods

All chemicals obtained commercially were of analytical grade and used without further purification. No-carrier-added ^{18}F-F^- was obtained from an in-house PETtrace cyclotron (GE Healthcare). The syringe filter and polyethersulfone membranes (pore size, 0.22 μm; diameter, 13 mm) were obtained from Nalge Nunc Internationals. ^{125}I-Echistatin, labeled by the lactoperoxidase method to a specific activity of 74 TBq/mmol (2,000 Ci/mmol) was purchased from GE healthcare. The peptides c(RGDfK) (denoted as RGDfK), c(RGDyK) (denoted as RGDyK), E[c(RGDyK)]$_2$ (denoted as RGD2), and PEG3-E [c(RGDyK)]$_2$ (denoted as PRGD2) were synthesized by Peptides International. The semipreparative reversed-phase high-performance liquid chromatography (HPLC) using a Vydac protein and peptide column (218TP510; 5 μm, 250×10 mm) was performed on a Dionex 680 chromatography system with a UVD 170U absorbance detector and model 105 S single-channel radiation detector (Carroll and Ramsey Associates). The recorded data were processed using Chromeleon version 6.50 software. With a flow rate of 5 mL/min, the mobile phase was changed from 95% solvent A [0.1% trifluoroacetic acid (TFA) in water] and 5% B [0.1% TFA in acetonitrile (MeCN)] (0–2 min) to 35% solvent A and 65% solvent B at 32 min. Analytical HPLC has the same gradient system except that the flow rate was 1 mL/min with a Vydac protein and peptide column (218TP510; 5 μm, 250×4.6 mm). The UV absorbance was monitored at 218 nm, and the identification of the peptides was confirmed based on the UV spectrum acquired using a PDA detector. C_{18} Sep-Pak cartridges (Waters) were pretreated with ethanol and water before use.

Synthesis of SAA-RGD Peptides

The synthesis of Fmoc-protected sugar amino acid (Fmoc-SAA-OH) was accomplished by a reported method [30]. As a typical procedure for all the Fmoc-SAA-RGD peptides, Fmoc-SAA-RGD2 was synthesized as follows: to a solution of Fmoc-SAA-OH (4.3 mg, 10 μmol) in 0.5 mL *N*,*N*′-dimethylformamide (DMF) was added *O*(*N*-succinimidyl)-1,1,3,3-tetramethyluronium tetrafluoroborate (TSTU; 2.4 mg, 8 μmol) and 20 μL *N*,*N*-diisopropylethylamine (DIPEA). After incubating at room temperature for 30 min, RGD2 (2 μmol) in 200 μL dimethyl sulfoxide (DMSO) was loaded in one aliquot. The reaction was stirred at room temperature for 2 h, and the product Fmoc-SAA-RGD2 was isolated by semipreparative HPLC. The collected fractions were combined and lyophilized to give a white fluffy powder. The Fmoc group was readily removed by treating Fmoc-SAA-RGD2 with 20% piperidine in DMF for 30 min at ambient temperature. After dilution with 0.5 mL 1% TFA, the mixture was purified by semipreparative HPLC. The desired fractions containing SAA-RGD2 were combined and lyophilized to afford SAA-RGD2 as white powder. SAA-c(RGDfK) (denoted as SAA-RGDfK) was obtained in 74% yield with 10.2 min retention time on analytical HPLC. Matrix-assisted laser desorption/ionization time-of-flight mass spectrometry (MALDI-TOF-MS) was *m*/*z* 793.9 for $[MH]^+$ ($C_{34}H_{53}N_{10}O_{12}$, calculated molecular weight 793.8). SAA-c(RGDyK) (denoted as SAA-RGDyK) was obtained in 65% yield with 10.0-min retention time on analytical HPLC. MALDI-TOF-MS was *m*/*z* 809.7 for $[MH]^+$ ($C_{34}H_{53}N_{10}O_{13}$, calculated molecular weight 809.8). SAA-E[c(RGDyK)]$_2$ (denoted as SAA-RGD2) was obtained in 45% yield with 12.6 min retention time on analytical HPLC. MALDI-TOF-MS was *m*/*z* 1539.9 for $[MH]^+$ ($C_{66}H_{98}N_{20}O_{23}$, calculated molecular weight 1,539.6).

Synthesis of FP-SAA-c(RGDfK) (Denoted as Galacto-RGD), FP-SAA-c(RGDyK) (Denoted as FP-SRGDyK), FP-SAA-RGD2 (Denoted as FP-SRGD2), and FP-PEG3-RGD2 (Denoted as FP-PRGD2)

As a typical procedure for all the FP-SAA-RGD peptides, FP-SRGD2 was synthesized as follows: to the solution of 2-fluoropropionic acid (7.8 mg, 84.5 μmol) in 0.5 mL anhydrous MeCN was added TSTU (17.6 mg, 58.5 μmol). The pH of the solution was adjusted to 8.5–9.0 by DIPEA. The reaction mixture was stirred at room temperature for 0.5 h, and then SRGD2 (3 μmol) in DMF was added in one aliquot. After being stirred at room temperature for 2 h, the product FP-SRGD2 was isolated by semipreparative HPLC. The collected fractions were combined and lyophilized to afford white fluffy powder. Galacto-RGD was obtained in 92% yield with 11.8-min retention time on analytical HPLC. MALDI-TOF-MS was *m*/*z* 868.1 for $[MH]^+$ ($C_{37}H_{56}FN_{10}O_{13}$, calculated molecular weight 867.9). FP-SRGDyK was obtained in 88% yield with 11.6-min retention time on analytical HPLC. MALDI-TOF-MS was *m*/*z* 883.7 for $[MH]^+$ ($C_{37}H_{56}FN_{10}O_{14}$, calculated molecular weight 883.9). FP-SRGD2 was obtained in 72% yield with 14.5-min retention time on analytical HPLC. MALDI-TOF-MS was *m*/*z* 1,614.9 for $[MH]^+$ ($C_{69}H_{102}FN_{20}O_{24}$, calculated molecular weight 1,614.7). FP-PRGD2 was obtained in 85% yield with 13.8-min retention time on analytical HPLC. MALDI-TOF-MS was *m*/*z* 1,616.2 for $[MH]^+$ ($C_{70}H_{106}FN_{20}O_{23}$, calculated molecular weight 1,614.7).

Preparation of FB-SAA-RGD2 (Denoted as FB-SRGD2)

N-Succinimidyl-4-fluorobenzoate (SFB; 2 mg, 8.4 μmol) and SRGD2 (1.0 mg, 0.6 μmol) were mixed in 0.05-M borate buffer (pH 8.5) at room temperature. After 2 h, the product FB-SRGD2 was isolated by semipreparative HPLC in 58% yield. Retention time on analytical HPLC was 15.2 min, and MALDI-TOF-MS *m*/*z* was 1,661.9 for $[MH]^+$ ($C_{73}H_{102}FN_{20}O_{24}$, calculated molecular weight 1,661.7).

Cell-Binding Assay

In vitro integrin $\alpha_v\beta_3$ receptor-binding affinity and specificity of galacto-RGD, FP-SRGDyK, FP-SRGD2, FP-PRGD2, and FB-SRGD2 were assessed via a competitive cell-binding assay using ^{125}I-echistatin as the integrin $\alpha_v\beta_3$-specific radioligand. Experiments were performed on U87MG human glioblastoma cells with triplicate samples, as previously reported [31,32]. The best-fit 50% inhibitory concentration (IC_{50}) values for the U87MG cells were calculated by fitting the data with nonlinear regression using GraphPad Prism (GraphPad Software, Inc.).

Radiochemistry

^{18}F-NFP was synthesized as previously reported with HPLC purification [30,33]. As a typical procedure for all the ^{18}F-FP-RGD peptides, ^{18}F-FP-SRGD2 was synthesized as follows: the HPLC-purified ^{18}F-NFP was rotary-evaporated to dryness, redis solved in DMSO (200 μL), and added to a solution of SRGD2 (1.0 μmol) and DIPEA (20 μL). The reaction mixture was allowed to incubate at 60°C for 30 min. After dilution with 2 mL of water and 0.1% TFA, the mixture was injected into the semipreparative HPLC. The collected fractions containing ^{18}F-FP-SRGD2 were combined and rotary-evaporated to remove MeCN and TFA (the radiochemical yields and radio-HPLC retention time were shown in the “Electronic Supplementary Materials”). The activity was then reconstituted in normal saline and passed through a 0.22-μm Millipore filter into a sterile multidose vial for *in vivo* experiments.

^{18}F-SFB was synthesized by an automated protocol developed in our research lab using a commercially available synthesis module (GE TRACERlab FX_{FN}; GE Healthcare; detailed procedure to be published elsewhere). The purified ^{18}F-SFB were rotary-evaporated to dryness, redissolved in DMSO (200 μL), and added to a solution of SRGD2 (1.0 μmol) and DIPEA (20 μL). The reaction mixture was allowed to incubate at 60°C for 30 min. After dilution with 2 mL of 0.1% TFA water, the mixture was injected into the semipreparative HPLC. The collected fractions containing ^{18}F-FB-SRGD2 were combined and rotary-evaporated to remove MeCN and TFA (the radiochemical yields and radio-HPLC retention time were shown in the “Electronic Supplementary Materials”). The activity was then reconstituted in normal saline and passed through a 0.22-μm Millipore filter into a sterile multidose vial for *in vivo* experiments.

Cell Line and Animal Model

U87MG human glioblastoma cells were grown in Dulbecco’s medium (Gibco, Carlsbad, CA, USA) supplemented with 10% fetal bovine serum, 100 IU/mL penicillin, and 100 μg/mL streptomycin (Invitrogen), at 37°C in a humidified atmosphere containing 5% CO_2. All animal experiments were performed under a protocol approved by Stanford’s Administrative Panel on Laboratory Animal Care. The U87MG tumor model was generated by injection of 5×10^6 cells in 50 μL PBS into the shoulder of female athymic nude mice (Harlan, Indianapolis, IN, USA). The mice were subjected to small-animal PET studies when the tumor volume reached 100–300 mm^3 (3–4 weeks after inoculation).

Small-Animal PET Imaging

PET scans and image analysis were performed using a microPET R4 rodent model scanner (Siemens Medical Solutions) as previously reported [22]. Each mouse was tail-vein-injected with about 3.7 MBq (100 μCi) of ^{18}F-galacto-RGD, ^{18}F-FP-SRGDyK, ^{18}F-FP-SRGD2, ^{18}F-FP-PRGD2, or ^{18}F-FB-SRGD2 under isoflurane anesthesia. Five-minute static PET images were acquired at 20 min, 1, and 2 h postinjection (p.i.; *n*=4/group). The images were reconstructed by a two-dimensional ordered-subsets expectation maximum algorithm, and

no correction was applied for attenuation or scatter. For the blocking experiments, the tumor-bearing mice were coinjected with 10-mg/kg mouse body weight of c(RGDyK) and 3.7 MBq of ^{18}F-FP-SRGD2 or ^{18}F-FP-PRGD2, and 5-min static PET scans were then acquired at 20 min, 1, and 2 h p.i. (n=3/group). For each microPET scan, regions of interest (ROIs) were drawn over the tumor, normal tissue, and major organs by using vendor software (ASI Pro 5.2.4.0; Siemens Medical Solutions) on decay-corrected whole-body coronal images. The maximum radioactivity concentration (accumulation) within a tumor or an organ was obtained from mean pixel values within the multiple ROI volume, which were converted to counts per milliliter per minute by using a conversion factor. Assuming a tissue density of 1 g/mL, the ROIs were converted to counts per gram per minute and then divided by the administered activity to obtain an imaging ROI-derived percentage injected dose per gram tissue (%ID/g).

Statistical Analysis

Quantitative data were expressed as mean ± SD. Means were compared using one-way analysis of variance and Student's t test. P value of <0.05 was considered statistically significant.

Results

Chemistry and Radiochemistry

The synthesis of Fmoc-SAA-OH started with penta-*O*-acetylgalacto-β-D-pyranose. The anomeric acetyl group was readily replaced with cyanide in the presence of trimethylsilyl cyanide and boron trifluoride with a yield of 75%. The cyanide group was reduced with $LiAlH_4$ in dry THF, and at the same time, all the rest of acetyls were removed. Without further purification, the newly formed amine was protected with Fmoc chloride under a slightly basic condition. After oxidation, the desired Fmoc-SAA-OH was obtained in a yield of 77%. Before being coupled with the peptides, Fmoc-SAA-OH was activated with TSTU/DIPEA and then conjugated with the amino group of different RGD peptides under a slightly basic condition. After piperidine deprotection, the SAA-RGD peptides were obtained as a white fluffy powder ready for radiolabeling.

The total synthesis time for ^{18}F-NFP was about 70 min including an HPLC purification of the active ester. The total synthesis time for ^{18}F-SFB was about 90 min. The decay-corrected radiochemical yields for ^{18}F-FP-SRGD2 and ^{18}F-FP-PRGD2 based on ^{18}F-NFP were 52±9% (n=5) and 80± 7% (n=5), respectively. The radiochemical purity of all the radiotracers was more than 99% and chemical purity over 90% according to analytical HPLC. The specific radioactivity of ^{18}F-FP-PRGD2 was determined to be more than 37 TBq/mmol at the end of synthesis. For all the labeling, the unlabeled cold peptides were efficiently separated from the products. Starting from ^{18}F-F^-, the total synthesis time of each ^{18}F-FP-RGD tracer was about 120 min, and the overall decay-corrected yields ranged from 8% to 56% for different RGD peptides (Fig. 1), and the total synthesis time for ^{18}F-FB-SRGD2 tracer was about 110 min with the overall decay-corrected yields range from 8% to 12% ("Electronic Supplementary Material").

In vitro Cell Integrin Receptor-Binding Assay

The receptor-binding affinity of galacto-RGD, FP-SRGDyK, FP-SRGD2, FP-PRGD2, and FB-SRGD2 was determined by performing competitive displacement studies with ^{125}I-echistatin. All peptides inhibited the binding of ^{125}I-echistatin (integrin $\alpha_v\beta_3$ specific) to U87MG cells in a concentration-dependent manner. The IC_{50} values for galacto-RGD, FP-SRGDyK, FP-SRGD2, FP-PRGD2, and FB-SRGD2 were 404±38, 485±42, 79.6±8.8, 51.8±4.6, and 60.2±5.4 nM (n=3, mean ± SD; Fig. 2). Overall, the monomeric RGD

peptides galacto-RGD and FP-SRGDyK possessed comparable affinity, and the dimeric RGD peptides FP-SRGD2, FP-PRGD2, and FB-SRGD2 also showed similar receptor-binding affinity. Due to the polyvalency effect, RGD dimers have much higher integrin $\alpha_v\beta_3$ binding affinity than the RGD monomers.

MicroPET Imaging Studies on Tumor-Bearing Mice

The tumor-targeting efficacy of ^{18}F-galacto-RGD, ^{18}F-FP-SRGDyK, ^{18}F-FP-SRGD2, ^{18}F-FP-PRGD2, and ^{18}F-FB-SRGD2 in U87MG tumor-bearing nude mice was evaluated by static microPET scans. The representative decay-corrected coronal images at different time points after injection of the radiotracers were shown in Fig. 3a, b. The U87MG tumors were clearly visualized with good tumor-to-background contrast for all the tracers at 20 min p.i. The tumor signals of the monomeric RGD tracers (^{18}F-galacto-RGD, and ^{18}F-FP-SRGDyK) were weaker than those of the dimeric RGD tracers (^{18}F-FP-SRGD2, ^{18}F-FP-PRGD2, and ^{18}F-FB-SRGD2; Fig. 3a, b). Quantitation of tumor and major organ activity accumulation was performed by measuring ROIs encompassing the entire organ on the coronal images. The uptake of all five tracers in the tumor, liver, kidneys, and muscle at different time points p.i. were shown in Table 1. The monomeric RGD tracers, ^{18}F-galacto-RGD and ^{18}F-FP-SRGDyK, had moderate tumor uptake, which was determined to be 2.1±0.2, 1.2±0.1, and 0.9± 0.1%ID/g for ^{18}F-galacto-RGD and 1.9 ± 0.2, 1.5±0.2, and 1.0±0.1%ID/g for ^{18}F-FP-SRGDyK at 20, 60, and 120 min p.i., respectively. The U87MG tumor uptake of ^{18}F-FP-SRGD2 was calculated to be 4.3±0.4, 2.8±0.4, and 2.1± 0.2%ID/g at 20, 60, and 120 min p.i., which was significantly higher than those of the two monomeric RGD tracers at any time examined (P<0.01). All five tracers showed predominant renal clearance and minimal hepatobiliary excretion, which was evidenced by the high initial kidney uptake and very low activity accumulation in the intestines (Fig. 3a, b). The ^{18}F-FP-SRGD2 had twice as much tumor uptake and similar tumor-to-background ratio compared to the monomeric analogs. Both ^{18}F-FP-SRGD2 and ^{18}F-FP-PRGD2 showed integrin specificity *in vivo* as indicated in Fig. 3c. The *in vivo* behavior of the PEGylated tracer ^{18}F-FP-PRGD2 proved to be similar to that of the galacto-linked ^{18}F-FP-SRGD2 tracers without significant difference in tumor uptake and *in vivo* kinetics (Fig. 4). The tumor uptake of ^{18}F-FB-SRGD2 was calculated to be 4.2±0.2, 2.3±0.3, 1.7±0.3%ID/g at 20, 60, and 120 min p.i., indicating slightly more rapid tumor washout than 2-^{18}F-fluoropropionate labeled RGD dimer analogs. The tumor-to-background ratios of ^{18}F-FB-SRGD2 were much lower than those of the other two dimeric analogs (Fig. 4). For better illustration of the tumor-targeting efficiency and favorable pharmacokinetics of ^{18}F-FP-PRGD2, a 2D projection image and 3D mpg movie file at 1-h time point were shown in the “Electronic Supplementary Material.”

Biodistribution Studies and Blocking Experiment

To investigate the localization of the dimeric probes, ^{18}F-FP-SRGD2 and ^{18}F-FP-PRGD2, in U87MG tumor-bearing nude mice, we performed biodistribution studies at 1 h p.i. with or without a blocking dose of c(RGDyK; Fig. 5). As can be seen in this figure, the uptake values of ^{18}F-FP-SRGD2 and ^{18}F-FP-PRGD2 in the kidneys were 2.7±0.4 and 2.5±0.4% ID/g (n=3/group), respectively, and the uptake values of ^{18}F-FP-SRGD2 and ^{18}F-FP-PRGD2 in the tumor were 2.1± 0.2 and 2.3±0.2%ID/g (n=3/group), respectively. The biodistribution results correlated well with the microPET data. The other organs had background-level activity accumulation. A coinjection of excess amount of c(RGDyK) successfully reduced the uptake of both ^{18}F-FP-SRGD2 and ^{18}F-FP-PRGD2 in U87MG tumors, confirming the integrin $\alpha_v\beta_3$-binding specificity *in vivo*. Similar to the previously observed results, the tracer cleared from the body significantly faster, and the uptake in most of the organs (e.g., liver, kidneys, and muscle) was also lower than those without c(RGDyK) blocking [34,35].

Discussion

Because extracellular matrix (ECM) proteins such as vitronectin, fibrinogen, and fibronectin interact with integrin via the RGD sequence, both linear and cyclic RGD peptides have been introduced as $\alpha_v\beta_3$-specific ligands. The penta-peptide cyclo(-Arg-Gly-Asp-D-Phe-Val-) shows high affinity and selectivity for $\alpha_v\beta_3$, and it became the most prominent structure for the development of molecular imaging compounds for the determination of $\alpha_v\beta_3$ expression [36]. Although the receptor-specific tumor uptake was confirmed, the relatively high activity concentration in liver and intestine is unfavorable for patient studies [37]. One strategy to improve the pharmacokinetics of radiolabeled peptides is to conjugate the cyclic pentapeptide RGD with glucose- or galactose-based sugar amino acids, leading to predominant renal elimination and increased uptake and retention in a murine tumor model compared with the first-generation peptides [12]. The tumor-to-background ratio calculated from small-animal PET images was comparable due to the faster elimination. PEGylation is another way to improve the pharmacokinetics of peptides [38]. The different effects of PEGylation on the pharmacokinetics, tumor uptake, and retention time depend strongly on the nature of the peptide structures as well as the size of the PEG moiety [39,40]. Although with good tumor contrast, the absolute tumor uptake value was not satisfactory due to the relatively low receptor-binding affinity of the RGD monomers. The use of multimeric cyclic RGD peptides to improve the integrin $\alpha_v\beta_3$ binding affinity was based on the fact that the interaction between integrin $\alpha_v\beta_3$ and RGD-containing ECM proteins involves multivalent binding sites with clustering of integrins [41]. Previous reports of dimers, tetramers, and octamers showed that the increase of binding affinity to $\alpha_v\beta_3$ integrin led to improved tumor uptake [22,25,26,42]. Polyvalency effect is more obvious in low- to medium-integrin-expressing tumors than high-integrin-expressing ones. However, high affinity originated from the multimeric RGD was also accompanied with high background, prolonged circulation half-life, and incredibly high kidney uptake attributed to nonnegligible integrin level in the normal organs and tissues. Dimeric RGD peptides with much higher receptor binding than the monomeric analogs and relatively low background are thus the focus of this study.

2-Fluoroacetate is the smallest possible fluorocarboxylic acid. However, the low *in vivo* stability greatly limited the application of 2-^{18}F-fluoroacetate as a prosthetic peptide radiolabeling agent. As a result, the 2-^{18}F-fluoropropionic acid (^{18}F-FP) is practically the smallest fluorocarboxylic acid useful for ^{18}F-labeling of bioactive molecules with primary amine functionalities. This study described the synthesis of ^{18}F-FP-labeled RGD monomers and dimers with galacto or PEG_3 spacer. For comparison purpose, 4-^{18}F-fluorobenzoate (^{18}F-FB)-labeled SRGD2 was also synthesized and characterized.

A cell-binding assay using integrin-positive U87MG cells and ^{125}I-echistatin as the radioligand found that integrin binding affinity of the dimeric tracers (^{18}F-FP-SRGD2, ^{18}F-FP-PRGD2, and ^{18}F-FB-SRGD2) was higher than those of the monomeric analogs (^{18}F-galacto-RGD and ^{18}F-FP-SRGDyK; Fig. 2). The galacto and PEG_3 spacers as well as the prosthetic groups had minimal effect on the receptor binding of the RGD derivatives *in vitro*. When applied to the subcutaneous U87MG glioblastoma xenograft model which has high integrin $\alpha_v\beta_3$ expression, all the RGD peptide tracers showed predominant renal clearance. ^{18}F-FP-SRGD2 with galacto spacer had significantly higher uptake than ^{18}F-galacto-RGD and ^{18}F-FP-SRGDyK at all time points examined (Table 1). The tumor-to-background ratios of the dimers were slightly lower than the monomeric counterparts at early time points, but the difference was diminished with time. The PEGylated dimer ^{18}F-FP-PRGD2 had similar *in vitro* and *in vivo* behavior to the galacto dimer ^{18}F-FP-SRGD2; however, the radiolabeling yield of ^{18}F-FP-PRGD2 (80%) is substantially higher than that of ^{18}F-FP-SRGD2 (52%), probably due to the less steric hindrance of extended amino group

from the bulky peptide structure. Furthermore, the incorporation of galacto spacer requires the laborious four-step synthesis of Fmoc-SAA-OH; PEG_3 linker seems practically more useful and easily available. This result was also consistent with another PEGylated RGD dimeric tracer reported earlier [26]. ^{18}F-FB-SRGD2 was synthesized starting from ^{18}F-SFB with radiochemical yield of about 22%, which was much lower than that for ^{18}F-FP-SRGD2. The low radiochemical yield was mainly due to the challenge to purify the desired radiotracer from the decomposed products of ^{18}F-SFB. ^{18}F-FB-SRGD2 had similar tumor uptake and clearance profile with ^{18}F-FP-PRGD2 and ^{18}F-FP-SRGD2 but with lower tumor-to-background contrast. Taken together, ^{18}F-FP-PRGD2 with high synthetic yield, high and prolonged tumor retention, and good tumor-to-background ratio outperforms ^{18}F-galacto-RGD monomer and other dimeric RGD peptide tracers tested in this study.

Conclusion

^{18}F-FP-PRGD2 and ^{18}F-FP-SRGD2 were shown to bind with high affinity and specificity with integrin-positive U87MG glioma cells *in vitro* and *in vivo*. Although both tracers had higher tumor uptake than ^{18}F-galacto-RGD, the high radio-chemical yield and relatively easy purification procedure for ^{18}F-FP-PRGD2 allows for imaging integrin expression for cancer diagnosis and for treatment response monitoring. Indeed, the exploratory investigative new drug application for ^{18}F-FP-PRGD2 was recently approved by FDA (IND 104150) for first-in-human test. The side-by-side comparison of ^{18}F-FP-PRGD2 with ^{18}F-galacto-RGD in human is currently in progress.

Supplementary Material

Refer to Web version on PubMed Central for supplementary material.

Acknowledgments

This work was supported, in part, by the National Cancer Institute (R01 120188, R01 CA119053, R21 CA121842, P50 CA114747, U54 CA119367, and R24 CA93862). We thank the cyclotron team at Stanford University for $^{18}F^-$ production.

References

1. Bishop GG, McPherson JA, Sanders JM, Hesselbacher SE, Feldman MJ, McNamara CA, et al. Selective αvβ3-receptor blockade reduces macrophage infiltration and restenosis after balloon angioplasty in the atherosclerotic rabbit. Circulation 2001;103:1906–1911. [PubMed: 11294811]
2. Storgard CM, Stupack DG, Jonczyk A, Goodman SL, Fox RI, Cheresh DA. Decreased angiogenesis and arthritic disease in rabbits treated with an αvβ3 antagonist. J Clin Invest 1999;103:47–54. [PubMed: 9884333]
3. Teitelbaum SL. Bone resorption by osteoclasts. Science 2000;289:1504–1508. [PubMed: 10968780]
4. Albelda SM, Mette SA, Elder DE, Stewart R, Damjanovich L, Herlyn M, et al. Integrin distribution in malignant melanoma: association of the beta 3 subunit with tumor progression. Cancer Res 1990;50:6757–6764. [PubMed: 2208139]
5. Bello L, Francolini M, Marthyn P, Zhang J, Carroll RS, Nikas DC, et al. αvβ3 and αvβ5 integrin expression in glioma periphery. Neurosurgery 2001;49:380–389. [PubMed: 11504114]
6. Brooks PC, Stromblad S, Klemke R, Visscher D, Sarkar FH, Cheresh DA. Anti integrin αvβ3 blocks human breast cancer growth and angiogenesis in human skin. J Clin Invest 1995;96:1815–1822. [PubMed: 7560073]
7. Beer AJ, Schwaiger M. Imaging of integrin αvβ3 expression. Cancer Metastasis Rev 2008;27:631–644. [PubMed: 18523730]
8. Cai W, Niu G, Chen X. Imaging of integrins as biomarkers for tumor angiogenesis. Curr Pharm Des 2008;14:2943–2973. [PubMed: 18991712]

9. Dijkgraaf I, Beer AJ, Wester HJ. Application of RGD-containing peptides as imaging probes for αvβ3 expression. Front Biosci 2009;14:887–899. [PubMed: 19273106]
10. Cai W, Chen X. Multimodality molecular imaging of tumor angiogenesis. J Nucl Med 2008;49(Suppl 2):113S–128S. [PubMed: 18523069]
11. Chen X. Multimodality imaging of tumor integrin αvβ3 expression. Mini Rev Med Chem 2006;6:227–234. [PubMed: 16472190]
12. Haubner R, Wester HJ, Weber WA, Mang C, Ziegler SI, Goodman SL, et al. Noninvasive imaging of αvβ3 integrin expression using ^{18}F-labeled RGD-containing glycopeptide and positron emission tomography. Cancer Res 2001;61:1781–1785. [PubMed: 11280722]
13. Beer AJ, Haubner R, Sarbia M, Goebel M, Luderschmidt S, Grosu AL, et al. Positron emission tomography using [^{18}F]Galacto-RGD identifies the level of integrin αvβ3 expression in man. Clin Cancer Res 2006;12:3942–3949. [PubMed: 16818691]
14. Beer AJ, Haubner R, Wolf I, Goebel M, Luderschmidt S, Niemeyer M, et al. PET-based human dosimetry of ^{18}F-galacto-RGD, a new radiotracer for imaging αvβ3 expression. J Nucl Med 2006;47:763–769. [PubMed: 16644745]
15. Beer AJ, Niemeyer M, Carlsen J, Sarbia M, Nahrig J, Watzlowik P, et al. Patterns of αvβ3 expression in primary and metastatic human breast cancer as shown by ^{18}F-Galacto-RGD PET. J Nucl Med 2008;49:255–259. [PubMed: 18199623]
16. Picchio M, Beck R, Haubner R, Seidl S, Machulla HJ, Johnson TD, et al. Intratumoral spatial distribution of hypoxia and angiogenesis assessed by ^{18}F-FAZA and ^{125}I-Gluco-RGD autoradiography. J Nucl Med 2008;49:597–605. [PubMed: 18344437]
17. Beer AJ, Grosu AL, Carlsen J, Kolk A, Sarbia M, Stangier I, et al. [^{18}F]galacto-RGD positron emission tomography for imaging of alphavbeta3 expression on the neovasculature in patients with squamous cell carcinoma of the head and neck. Clin Cancer Res 2007;13:6610–6616. [PubMed: 18006761]
18. Beer AJ, Haubner R, Goebel M, Luderschmidt S, Spilker ME, Wester HJ, et al. Biodistribution and pharmacokinetics of the αvβ3-selective tracer ^{18}F-galacto-RGD in cancer patients. J Nucl Med 2005;46:1333–1341. [PubMed: 16085591]
19. Beer AJ, Lorenzen S, Metz S, Herrmann K, Watzlowik P, Wester HJ, et al. Comparison of integrin αvβ3 expression and glucose metabolism in primary and metastatic lesions in cancer patients: a PET study using ^{18}F-galacto-RGD and ^{18}F-FDG. J Nucl Med 2008;49:22–29. [PubMed: 18077538]
20. Haubner R, Weber WA, Beer AJ, Vabuliene E, Reim D, Sarbia M, et al. Noninvasive visualization of the activated αvβ3 integrin in cancer patients by positron emission tomography and [^{18}F]Galacto-RGD. PLoS Med 2005;2:e70. [PubMed: 15783258]
21. Kreiner M, Li Z, Beattie J, Kelly SM, Mardon HJ, van der Walle CF. Self-assembling multimeric integrin α5β1 ligands for cell attachment and spreading. Protein Eng Des Sel 2008;21:553–560. [PubMed: 18515822]
22. Zhang X, Xiong Z, Wu Y, Cai W, Tseng JR, Gambhir SS, et al. Quantitative PET imaging of tumor integrin αvβ3 expression with ^{18}F-FRGD2. J Nucl Med 2008;47:113–121. [PubMed: 16391195]
23. Chen X, Liu S, Hou Y, Tohme M, Park R, Bading JR, et al. MicroPET imaging of breast cancer αv-integrin expression with ^{64}Cu-labeled dimeric RGD peptides. Mol Imaging Biol 2004;6:350–359. [PubMed: 15380745]
24. Mammen M, Chio S-K, Whitesides GM. Polyvalent interactions in biological systems: implications for design and use of multivalent ligands and inhibitors. Angew Chem Int Ed Engl 1998;37:2755–2794.
25. Li ZB, Cai W, Cao Q, Chen K, Wu Z, He L, et al. ^{64}Cu-labeled tetrameric and octameric RGD peptides for small-animal PET of tumor αvβ3 integrin expression. J Nucl Med 2007;48:1162–1171. [PubMed: 17574975]
26. Wu Z, Li ZB, Cai W, He L, Chin FT, Li F, et al. ^{18}F-labeled mini-PEG spacered RGD dimer (^{18}F-FPRGD2): synthesis and micro-PET imaging of αvβ3 integrin expression. Eur J Nucl Med Mol Imaging 2007;34:1823–1831. [PubMed: 17492285]

27. Wu Z, Li ZB, Chen K, Cai W, He L, Chin FT, et al. microPET of tumor integrin αvβ3 expression using ^{18}F-labeled PEGylated tetrameric RGD peptide (^{18}F-FPRGD4). J Nucl Med 2007;48:1536–1544. [PubMed: 17704249]
28. Poethko T, Schottelius M, Thumshirn G, Hersel U, Herz M, Henriksen G, et al. Two-step methodology for high-yield routine radio-halogenation of peptides: ^{18}F-labeled RGD and octreotide analogs. J Nucl Med 2004;45:892–902. [PubMed: 15136641]
29. Thumshirn G, Hersel U, Goodman SL, Kessler H. Multimeric cyclic RGD peptides as potential tools for tumor targeting: solid-phase peptide synthesis and chemoselective oxime ligation. Chemistry 2003;9:2717–2725. [PubMed: 12772286]
30. Haubner R, Kuhnast B, Mang C, Weber WA, Kessler H, Wester HJ, et al. [^{18}F]Galacto-RGD: synthesis, radiolabeling, metabolic stability, and radiation dose estimates. Bioconjug Chem 2004;15:61–69. [PubMed: 14733584]
31. Cai W, Zhang X, Wu Y, Chen X. A thiol-reactive ^{18}F-labeling agent, *N*-[2-(4-^{18}F-fluorobenzamido)ethyl]maleimide, and synthesis of RGD peptide-based tracer for PET imaging of αvβ3 integrin expression. J Nucl Med 2006;47:1172–1180. [PubMed: 16818952]
32. Wu Y, Zhang X, Xiong Z, Cheng Z, Fisher DR, Liu S, et al. microPET imaging of glioma integrin αvβ3 expression using ^{64}Cu-labeled tetrameric RGD peptide. J Nucl Med 2005;46:1707–1718. [PubMed: 16204722]
33. Liu Z, Liu S, Wang F, Chen X. Noninvasive imaging of tumor integrin expression using ^{18}F-labeled RGD dimer peptide with PEG_4 linkers. Eur J Nucl Med Mol Imaging 2009;36:1296–1307. [PubMed: 19296102]
34. Dijkgraaf I, Kruijtzer JA, Liu S, Soede AC, Oyen WJ, Corstens FH, et al. Improved targeting of the αvβ3 integrin by multimerisation of RGD peptides. Eur J Nucl Med Mol Imaging 2007;34:267–273. [PubMed: 16909226]
35. Janssen ML, Oyen WJ, Dijkgraaf I, Massuger LF, Frielink C, Edwards DS, et al. Tumor targeting with radiolabeled αvβ3 integrin binding peptides in a nude mouse model. Cancer Res 2002;62:6146–6151. [PubMed: 12414640]
36. Haubner R, Finsinger D, Kessler H. Stereoisomeric peptide libraries and peptidomimetics for designing selective inhibitors of the αvβ3 integrin for a new cancer therapy. Angew Chem Int Ed Engl 1997;36:1374–1389.
37. Haubner R, Wester HJ, Reuning U, Senekowitsch-Schmidtke R, Diefenbach B, Kessler H, et al. Radiolabeled αvβ3 integrin antagonists: a new class of tracers for tumor targeting. J Nucl Med 1999;40:1061–1071. [PubMed: 10452325]
38. Harris JM, Martin NE, Modi M. Pegylation: a novel process for modifying pharmacokinetics. Clin Pharmacokinet 2001;40:539–551. [PubMed: 11510630]
39. Chen X, Park R, Shahinian AH, Bading JR, Conti PS. Pharmacokinetics and tumor retention of ^{125}I-labeled RGD peptide are improved by PEGylation. Nucl Med Biol 2004;31:11–19. [PubMed: 14741566]
40. Schipper ML, Iyer G, Koh AL, Cheng Z, Ebenstein Y, Aharoni A, et al. Particle size, surface coating, and PEGylation influence the biodistribution of quantum dots in living mice. Small 2008;5:126–134. [PubMed: 19051182]
41. Boturyn D, Coll JL, Garanger E, Favrot MC, Dumy P. Template assembled cyclopeptides as multimeric system for integrin targeting and endocytosis. J Am Chem Soc 2004;126:5730–5739. [PubMed: 15125666]
42. Li ZB, Chen K, Chen X. ^{68}Ga-labeled multimeric RGD peptides for microPET imaging of integrin αvβ3 expression. Eur J Nucl Med Mol Imaging 2008;35:1100–1108. [PubMed: 18204838]

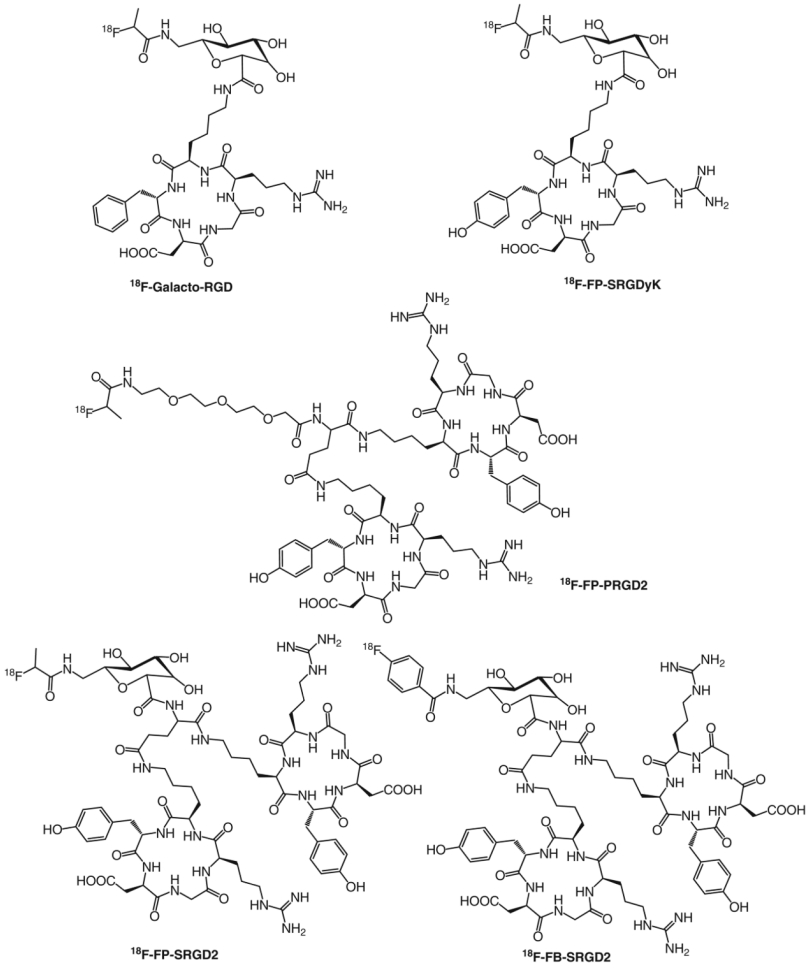

Fig. 1.
Chemical structures of ^{18}F-FP- and ^{18}F-FB-labeled RGD peptides

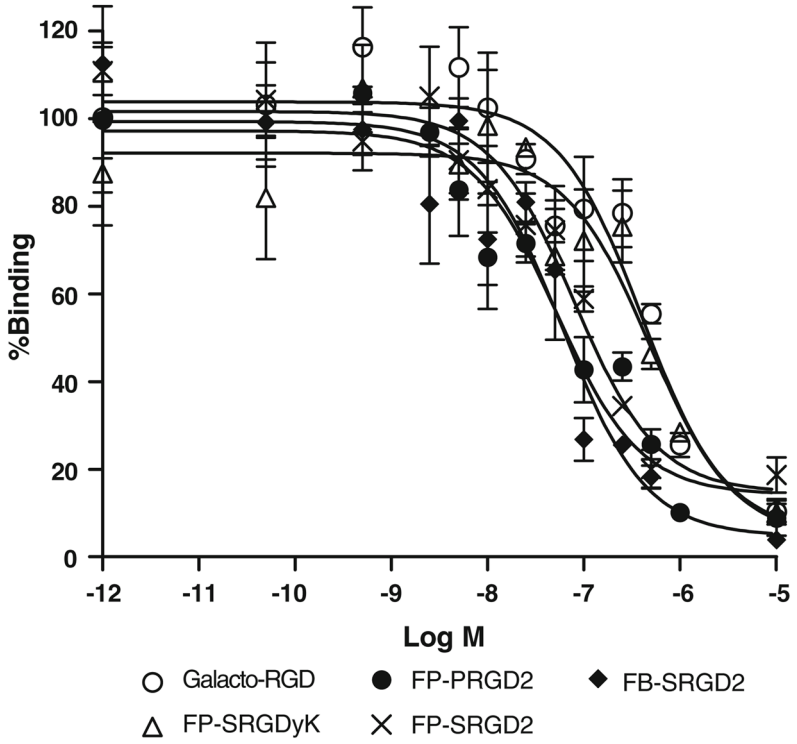

Fig. 2.

Inhibition of ^{125}I-echistatin binding to $\alpha_v\beta_3$ integrin on U87MG cells by galacto-RGD, FP-SRGDyK, FP-PRGD2, FP-SRGD2, and FB-SRGD2

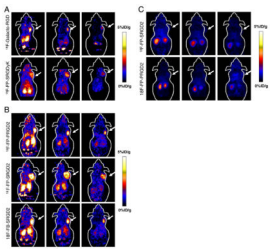

Fig. 3.

Small-animal PET images of U87MG tumor-bearing mice. **a** Decay-corrected whole-body coronal images at 20 min, 1, and 2 h after injection of about 3.7 MBq of ^{18}F-galacto-RGD and ^{18}F-FP-SRGDyK. **b** Decay-corrected whole-body coronal images at 20 min, 1, and 2 h after injection of about 3.7 MBq of ^{18}F-FP-SRGD2, ^{18}F-FP-PRGD2, and ^{18}F-FB-SRGD2. **c** Decay-corrected whole-body coronal images at 1 h after injection of about 3.7 MBq of ^{18}F-FP-SRGD2 and ^{18}F-FP-PRGD2 with coinjection of 10 mg c(RGDyK) per kilogram of mouse body weight

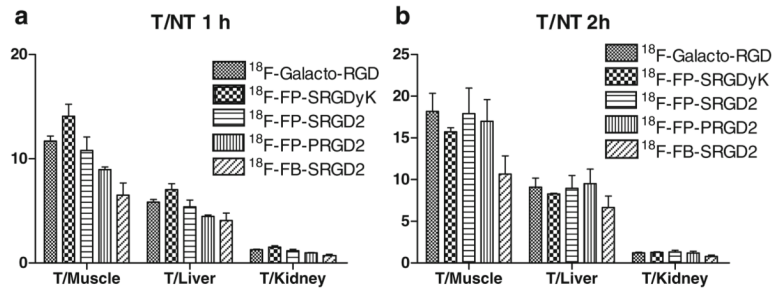

Fig. 4.

Comparison of tumor (*T*) to muscle, kidney, and liver ratios of five tracers at 1 h (**a**) and 2 h (**b**), respectively, after injection to U87MG tumor-bearing mice (*n*=3 per group, mean ± SD)

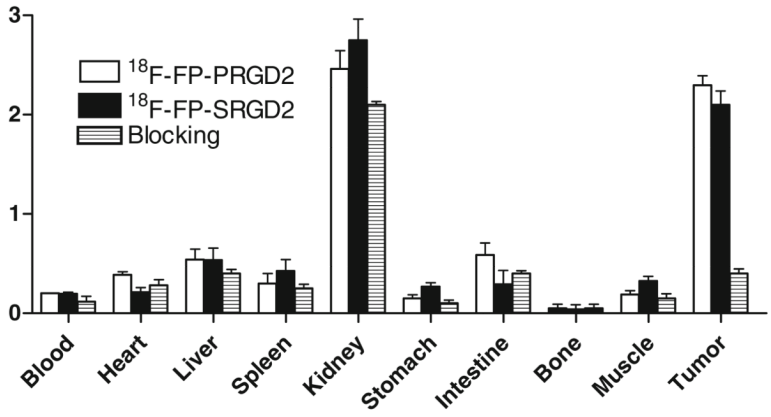

Fig. 5.

Biodistribution of ^{18}F-FP-PRGD2, ^{18}F-FP-SRGD2, and ^{18}F-FP-PRGD2 with coinjection of 10 mg/kg c(RGDyK) in female athymic nude mice bearing subcutaneous U87MG tumors at 1 h postinjection (*n*=3 per group)

Table 1

Uptake of different radiolabeled tracers in U87MG tumor, kidneys, liver, and muscle derived from PET quantification

	Time p.i. (min)	^{18}F-Galacto-RGD% ID/g ± SD	^{18}F-FP-SRGDyK% ID/g ± SD	^{18}F-FP-SRGD2% ID/g ± SD	^{18}F-FP-PRGD2% ID/g ± SD	^{18}F-FB-SRGD2% ID/g ± SD
Kidney	20	1.61±0.07	1.91±0.29	4.48±0.81	4.81±0.80	4.32±0.48
	60	0.91±0.08	0.96±0.15	2.48±0.63	2.88±0.42	3.40±0.58
	120	0.71±0.04	0.82±0.13	1.68±0.32	2.19±0.57	2.41±0.82
Liver	20	0.40±0.02	0.48±0.07	1.12±0.20	1.20±0.21	0.86±0.10
	60	0.20±0.02	0.21±0.03	0.54±0.14	0.63±0.09	0.59±0.10
	120	0.10±0.01	0.12±0.01	0.25±0.05	0.28±0.08	0.28±0.10
Muscle	20	0.20±0.01	0.24±0.04	0.56±0.10	0.60±0.10	0.54±0.06
	60	0.10±0.01	0.10±0.02	0.27±0.07	0.31±0.05	0.37±0.06
	120	0.05±0.01	0.07±0.01	0.12±0.02	0.15±0.04	0.18±0.06
Tumor	20	2.11±0.17	1.95±0.25	4.26±0.35	4.73±0.47	4.18±0.21
	60	1.16±0.06	1.47±0.23	2.82±0.39	2.80±0.46	2.32±0.28
	120	0.87±0.13	1.03±0.12	2.13±0.17	2.50±0.17	1.75±0.25

Mol Imaging Biol. Author manuscript; available in PMC 2010 December 8.